A Mesoscopic Numerical Study of Sea Ice Crystal Growth and Texture Development

Yoshiki Kawano, Tetsuya Ohashi

PII: S0165-232X(09)00020-2
DOI: doi: 10.1016/j.coldregions.2009.02.001
Reference: COLTEC 1369

To appear in: *Cold Regions Science and Technology*

Received date: 23 June 2008
Accepted date: 2 February 2009

Please cite this article as: Kawano, Yoshiki, Ohashi, Tetsuya, A Mesoscopic Numerical Study of Sea Ice Crystal Growth and Texture Development, *Cold Regions Science and Technology* (2009), doi: 10.1016/j.coldregions.2009.02.001

A Mesoscopic Numerical Study of Sea Ice Crystal Growth and Texture Development

Yoshiki Kawano and Tetsuya Ohashi

Dept. of Mechanical Engineering, Kitami Institute of Technology, 165, Koencho, Kitami, Hokkaido 090-8507, Japan

tel./fax.: +81-(0)157-26-9227

E-mail address: kawa@newton.kitami-it.ac.jp (Y. Kawano), Ohashi@newton.kitami-it.ac.jp (T. Ohashi)

Abstract

Development of sea ice polycrystals is simulated in two and three dimensions by a simple and efficient simulation technique, so-called Voronoi dynamics. First, effects of salt diffusion and heat flux are ignored and mutual impingements of stellar-shaped crystals are simulated in three-dimensional space. The simulated crystal texture and its c-axes distribution as a function of depth from the sea surface are shown to be in good agreement with experimental results. Next, three simulations are performed with different sets of parameters for growth rate in the basal plane. The obtained results show that geometrical selection of c-axes is more significant in weak anisotropy of growth rate in the basal plane than in strong anisotropy in the basal plane. However, the effect of the anisotropy on geometrical selection is modest. Effects of salt diffusion with time and salt rejection from growing ice to the ice-seawater interface as well as ocean heat flux are then incorporated into two-dimensional simulations. The results show that grains branch into thin ice platelets due to the relatively slow diffusion process during their growth. When the effect of heat flux is taken into consideration,

the platelets align in the vertical direction, and homogeneous columnar ice is formed. These results are in accordance with microstructural features of real sea ice.

Key Words: Sea ice; Development of Microstructure; Geometrical selection; Temperature Gradient; Instability of solid-liquid interface; Numerical simulation

1. Introduction

When seawater freezes, most of its salt content is rejected from the growing ice and is concentrated into the remaining liquid because the solubility limit of salt in the ice crystal lattice is very small. Thus, small volumes of saline solution, called brine inclusions or brine pockets, and air pores remain within ice crystals and at grain boundaries. Some physical properties of sea ice are closely linked to the microstructure of such ice crystals. For example, the strength of sea ice is affected by the volume fraction and distribution of brine inclusions as well as the shape and size of grains and temperature. Assur (1958) developed a pore microstructural model of sea ice and analyzed the relationship between the brine volume and macroscopic strength of sea ice, with the yield stress of macroscopic sea ice being given by a simple function of porosity.

A single ice crystal has a strong anisotropy in mechanical properties (Schulson, 1999), while polycrystalline sea ice may also show strong anisotropy depending on the degree of alignment of c-axes (Cole, 2001). Recently, Moslet (2007) conducted field experiments on uniaxial compression of sea ice, and their results showed sea ice that has substantial strength with higher porosities than suggested by Timco and Frederking (1990). However, the degree of alignment of c-axes was not taken into consideration in their experiment, and further study on the potential role of crystal alignment is therefore needed.

Fluid flow through sea ice is another point of interest. Permeability of sea ice is important in many physical processes such as drainage of meltwater from the surface of

sea ice during the melt season (Freitag and Eicken, 2003), transport of dissolved matter to the biological sea ice community (Cota et al., 1987) and heat flux with the movement of melt (Eicken et al., 2002). The relationship between porosity and permeability of sea ice has been studied (Golden et al., 1998, 2007). By using a Monte Carlo percolation model, Golden et al. (1998) showed that there is a strongly non-linear decrease in permeability of sea ice as brine volume fractions drop below 5%.

As mentioned above, properties of sea ice are changed by various factors such as volume fraction and distribution of brine inclusion and crystal orientation. However, there is a lack of data on the impact of these microstructural variables on the properties of sea ice. A numerical model that is capable of reproducing key aspects of sea ice microstructure as a function of environmental conditions may be useful for understanding how ice properties depend on microstructure, particularly alignment of c-axes.

The growth process of ice crystals has been studied at an atomistic level through molecular dynamics simulations (Noda et al., 2004), and the relationship between thickness and radius of an ice crystal growing in supercooled water has been analyzed by using a disc crystal model (Yokoyama and Sekerka, 2000). The formation and stability of cellular substructures for single crystals in NaCl solution were evaluated by Wettlaufer (1992). Experimental observations of the pattern formation of an ice crystal grown in supercooled water were also carried out (Shimada and Furukawa, 1997). In actual sea ice, the texture of growing crystals is affected by its neighboring crystals, and it differs from the texture of a single growing crystal in balk seawater. We define such a scale of a polycrystal level, which is larger than that of molecular and

single crystal level, not as microscopic but as mesoscopic, and we focused on the growth process, interaction of many ice crystals and the mechanism of formation of brine inclusions at the mesoscopic level with the aim of reproducing the growth process numerically.

We previously developed a simple numerical technique for simulating the process by which a sea ice crystal develops at a mesoscopic level, a technique we have named Voronoi dynamics (Ohashi et al., 2004), and the process by which a sea ice polycrystal structure develops was examined in two-dimensional approximation (Kawano and Ohashi, 2006a, 2006b). The crystal texture obtained by the simulations showed good agreement with real sea ice in terms of appearance. When crystal nuclei are introduced at the ocean's surface, a layer of granular ice typically develops, underlain by columnar-shaped grains. It has been reported that crystal orientation is random in the ice surface layer and that c-axes gradually align in the horizontal plane in the columnar-structured region (Weeks and Ackley, 1982, Weeks and Wettlaufer, 1996), while such transition could not be reproduced by the two-dimensional simulations.

In lake ice, the transition of c-axes with depth may differ from that of sea ice, and c-axis vertical orientations invariably can be observed depending on conditions (Gow, 1985). In sea ice, however, the c-axis alignment within the horizontal plane by geometrical selection commonly occurs due to the fact that growth rate in the direction perpendicular to c-axis is higher than that in the direction of c-axis. Although transition of crystal orientation in sea ice is well known (Weeks and Wettlaufer, 1996), little attention has been paid to the relationship between the magnitude of the anisotropy in the growth rate in the direction perpendicular to the c-axis and the process of c-axis

alignment.

Temperature gradient, which is generated by cooling from the sea surface, will also strongly affect the formation process of sea ice crystal. For example, the degree of supercooling of water near the ice-water interface is changed by change in the temperature gradient, and the change in supercooling affects the growth rate of crystal and its morphology (e.g. Shibcov, 2003). In the case of sea ice, change in growth rate affects the crystal texture, which has a characteristic cellular substructure consisting of evenly spaced ice plates or cells (Lofgren and Weeks (1969), Nakawo and Sinha (1981)). Growth rate dependence of the distance between adjacent plates or cells has been examined in NaCl ice (Lofgren and Weeks, 1969) and sea ice (Nakawo and Sinha, 1981). However, in the condition in which many nuclei are generated near the sea surface and grow and impinge, the effect of temperature gradient on the growth process has not been studied in detail.

In this study, we focused on the effect of growth rate anisotropy in the basal plane on c-axis fabric and the effect of temperature gradient on the process by which a polycrystal structure is formed in sea ice. In our previous model, the c-axis of nuclei was assumed to be normal to the two-dimensional simulation space, and growth rate anisotropy within normal to the basal plane could not be reproduced. First, we extended our previous work to simulate the development of polycrystalline ice texture in three dimensions, with only geometric effects governing the growth process and grain impingement. In the simulation, growth rate in the direction perpendicular to the c-axis (within the basal plane) was assumed to be higher than that in the c-axis direction. The resulting crystal microstructure and texture and c-axis fabrics are compared with

those of real sea ice samples. Furthermore, three simulations were performed with different anisotropy within the basal plane, and the relationship between the anisotropy and the transition process of the c-axis was examined. Next, the effects of salt and heat flux due to cooling from the sea surface were taken into account in two-dimensional simulations, and the development of a polycrystal texture as ice grows down from the sea surface was reproduced. The effect of temperature gradient on the texture of a growing polycrystal was examined.

2. Numerical procedure

2.1 Voronoi dynamics technique

Imagine a process in which crystals grow from nuclei and impinge on each other. During this process, crystals that have a faster growth rate and earlier nucleation time occupy larger areas than others. In order to reproduce such a process numerically, we use the following algorithm (Fig. 1).

Firstly, we assume a simulation space that is divided into small cells. All of the cells are initially given the character number -1, which means the cells are initially liquid (Fig. 1 (a)). Nuclei are put into the space and the positions of nuclei are determined arbitrarily except for the distance from a nucleus to its nearest neighbor, which is larger than the cell size. Each nucleus is given a certain growth rate $\boldsymbol{g}$, character number $\boldsymbol{k}$ and nucleation time. Cells that contain a nucleus are assumed to be solidified at the time of nucleation of the nucleus.

We advance the time and check whether growth from nuclei has reached each cell. If the growth of a nucleus with the character number $\boldsymbol{k}$ reaches the cell at time $\boldsymbol{t}$ and the conditions, **1)** the cell has the character number of liquid (-1) and **2)** at least one of the neighboring cells has the character number $\boldsymbol{k}$ are satisfied, the character number of the cell is changed from -1 to $\boldsymbol{k}$, which means the cell is solidified (Fig. 1 (b)). Then we advance the time from $\boldsymbol{t}$ to $\boldsymbol{t}+\boldsymbol{\Delta t}$ and the procedure described above is repeated, and solidification of cells progresses. The time increment $\boldsymbol{\Delta t}$ is set such that $\boldsymbol{\Delta t}$ × (maximum growth rate) is less than the minimum size of the cell. After a certain time, aggregates of solidified cells with the same character number are formed and each of

them is assumed to be an individual grain (Fig. 1 (c)).

In the procedure described above, crystals grow and aggregate as a result of competition for the unfrozen water volume between different nuclei. In the extreme case of an isotropic growth rate, simultaneous formation and growth of all nuclei and an initial salinity of zero, the resultant microstructure corresponds to a Voronoi polyhedron. Thus, we name the methodology Voronoi dynamics.

2.2 Salt concentration and depression of freezing point

In the Voronoi dynamics technique, only the geometrical effect by the mutual impingement of crystals is taken into account. However, in order to reproduce the growth process of an ice crystal in seawater, effects of salt on crystal growth must be taken into consideration in the model. In order to represent the process of salt rejection from the growing ice to the ice-seawater interface, we assume that salt in a solidified cell is equally distributed to its neighboring non-solidified cell(s) (Fig.2).

Increase in salt concentration impedes crystal growth by depression of freezing point. The relationship between salinity $\boldsymbol{S_b}$ and solidification temperature $\boldsymbol{T_s}$ of seawater is approximately given by a monotonically decreasing function of $\boldsymbol{S_b}$ (Eicken, 2003):

$$T_s = \frac{54.11 S_b}{S_b - 1000} + 273.15 \quad \left(250.15 \le T_s \le 273.15\right). \tag{1}$$

Liquid cells can solidify when the temperature is lower than the solidification point, and

the condition $T \le T_s$ should also be satisfied at cells for solidification.

2.3 Salt diffusion and conduction of heat

Diffusion of salt is expressed by Fick's Second Law:

$$\frac{\partial C_{salt}}{\partial t} = D\nabla^2 C_{salt}, \tag{2}$$

where C_{salt} and D denote concentration and diffusion coefficient of salt, respectively. The diffusion process of salt occurs only between liquid cells. Temperature T is changes by conduction of heat, and temperature distribution is governed by the following equation:

$$\frac{\partial T}{\partial t} = a\nabla^2 T, \tag{3}$$

where a is thermal diffusivity. Eqs. (2) and (3) are discretized by using the same space grid as the one used for Voronoi dynamics and solved by the finite difference method with the forward Euler's time integration scheme. Physical constants for seawater and pure ice are used for liquid and solidified cells, respectively.

2.4 Model for growth rate

Ice crystals of a hexagonal close-packing (hcp) lattice have a six-fold rotational symmetry in the basal plane, and the crystallographic properties in the normal to basal

plane (c-axis) also differ from those on the basal plane, and growth rate of ice is anisotropic. For the expression of such anisotropic growth characteristics, we use the following models of growth rate of nuclei in two- and three-dimensional simulations.

In the two-dimensional model, we assume that the c-axis of nuclei is normal to the simulation space and the growth rate in the basal plane is expressed by the following equation:

$$\boldsymbol{g}_{2d}^{(k)}(\theta) = \boldsymbol{g}_0 + \boldsymbol{g}_{ax} \times \cos\left(\boldsymbol{n}_s\theta + \alpha^{(k)}\right), \tag{4}$$

where $\boldsymbol{g_0}$ denotes the average growth rate and $\boldsymbol{g_{ax}}$ denotes the magnitude of deviation from the average. An integer number $\boldsymbol{n_s}$ defines the number of symmetricities, $\boldsymbol{\theta}$ denotes the growth direction, and $\boldsymbol{\alpha}$, which is given by a random number between 0 and 2π, defines the orientation of crystallites.

The magnitude of the growth rate anisotropy in the basal plane is defined by

$$\boldsymbol{R}_{anisotropy} = \frac{\boldsymbol{g}_{ax}}{\boldsymbol{g}_0}. \tag{5}$$

In three-dimensional simulations, the local coordinate system $\mathbf{x_0}$-$\mathbf{y_0}$-$\mathbf{z_0}$ is defined for each nucleus. Fig. 3 shows a schematic illustration of the coordinate system. Growth rate of nucleus $\boldsymbol{k}$ in the basal plane is expressed by

$$\boldsymbol{g}_{3d\ basal}^{(k)}\left(\theta_{basal}\right)=\boldsymbol{g}_0+\boldsymbol{g}_{ax}\times\cos\left(\boldsymbol{n}_s\theta_{basal}\right), \tag{6}$$

where $\boldsymbol{\theta}_{basal}$ is the angle between $\mathbf{x_0}$ and the vector of $\boldsymbol{g}_{3d\ basal}$ in the $\mathbf{x_0}$-$\mathbf{z_0}$ plane. Growth rate in the c-axis direction is assumed to be

$$\boldsymbol{g}_{3d\ c}^{(k)}=\boldsymbol{Const}. \tag{7}$$

Crystal orientation of each nucleus is determined by the rotation of the local coordinate system. The rotational relation between the local and global coordinate systems is defined by the Euler angle ($\boldsymbol{\varphi}_1^{(k)}$, $\boldsymbol{\varphi}_2^{(k)}$, $\boldsymbol{\varphi}_3^{(k)}$). Random numbers between 0 and 2π are generated and assigned to $\boldsymbol{\varphi}_1^{(k)}$, $\boldsymbol{\varphi}_2^{(k)}$ and $\boldsymbol{\varphi}_3^{(k)}$. Fig. 4 shows examples of shape of the crystals calculated by the above growth rate model when $\boldsymbol{R}_{anisotropy}$=0.5.

3. Results and discussion

3.1 Geometrical effect on crystal structure during growth

We examine anisotropic growth of crystals from the sea surface in three-dimensional space. Let us take a rectangular parallelepiped seawater region, which has the dimensions of 100×200×100 mm^3, and assume that the upper face of the region corresponds to the surface of the seawater.

Thirty points are randomly chosen near the surface as nucleation positions and they start to grow at t=0s. Values of g_0, g_c and g_{ax} are 1, 0.1 and 0.6×10^{-3} mm/s, respectively. With these parameters, crystals grow in dendrite shapes as shown in Fig. 4 (c) before their mutual impingements. The results of simulation are shown in Figs. 5 and 6.

Fig. 5 shows the development of crystal structure. In the initial growth period, crystal nuclei grow in dendrite shapes (Fig. 5 (a)), and they start to impinge mutually within the area in which nuclei are placed (Fig. 5 (b), (c)). After that, most of the nuclei stop growing due to the impingements, and they form relatively small grains near the sea surface (Fig. 5 (d)). After most of the volume near the sea surface is filled with grains, growth of grains that are in contact with the liquid region continues in the downward direction (Fig. 5 (e)) and a columnar-shaped structure is formed in the lower part of the specimen (Fig. 5 (f)). From these results, we find that the crystal structure is fine granular within the area in which nuclei are generated and columnar-shaped grains are formed in an area far from the nucleation position by the geometrical effect.

Next, we compare the obtained crystal structure with experimental ones. Sectional

views obtained from the final crystal structure (Fig. 5 (f)) are shown in Fig. 6. Fig. 6 (a) and (b) show vertical cross sections and Fig. 6 (c) show a horizontal cross section. Fig. 7 (Sasaki, 2003) shows the microstructure of artificially grown sea ice (see appendix for the experimental procedure). If we compare Fig. 8 with the structures shown in Fig. 6, we find that characteristics of the microstructure obtained by the simulation have good correspondence to characteristics of the microstructure obtained from artificially grown sea ice.

In the simulation, crystals tend to grow in a stellar-shaped disc, rather than a rod, because we assumed a growth rate condition $\boldsymbol{g_0} >> \boldsymbol{g_c}$. Thus, crystals with the c-axis horizontal are most likely to grow rapidly in the downward direction and occupy most of the volumes at a large depth. Hence, even if various orientations of ice crystals are possible near the ice surface in which the nuclei were initially introduced, the number of crystals with their c-axis within the horizontal plane increases in the lower part of the simulation space.

Next, orientation as a function of depth is studied through analysis of pole figures. The pole figures shown in Fig. 8 correspond to the simulated microstructure shown in Fig. 5 (f). The dots in Fig. 8 indicate the direction of the c-axis of individual crystals; a dot positioned near the center of the pole figure means a crystal is oriented with its c-axis directed nearly vertical, and a dot on the circumference means that the c-axis of the crystal is oriented horizontally.

At small depths, orientations of c-axes are random, whereas at 50 and 100 mm, the directions of c-axes tend to lie horizontally. This preferred alignment is caused by the

fact that the growth rate of nuclei in the direction vertical to the c-axis is higher than that in the c-axis direction, and geometrical selection occurs during their growth. As a result, c-axes are aligned horizontally at greater depth.

Changes in c-axis fabrics observed with depth in natural sea ice grown during a calm night, as reported by Weeks and Ackley (1982), are shown in Fig.9. Dark shading corresponds to a high density of c-axes at that particular orientation. The transition between random and highly aligned c-axis orientations at depths of a few centimeters (Fig. 9) is reproduced well by our simulation and can be explained by geometric selection.

In order to examine the above-mentioned geometrical selection of crystal orientation during crystal growth in more detail, three simulations are performed with different sets of parameters for growth rate. The number of crystal nuclei is increased from 30 to 300. Other conditions are the same as those used in the previous simulation. In the first simulation, parameters of growth rate are $\boldsymbol{g_0}$:$\boldsymbol{g_c}$: $\boldsymbol{g_{ax}}$=10:1:0 and disc-shaped crystals grow. In the second and third simulations, growth rate of crystals also exhibits anisotropy in the basal plane, and the initial shape of crystals is dendritic. The growth rate conditions are $\boldsymbol{g_0}$:$\boldsymbol{g_c}$:$\boldsymbol{g_{ax}}$=10:1:6 in the second simulation and $\boldsymbol{g_0}$:$\boldsymbol{g_c}$:$\boldsymbol{g_{ax}}$=10:1:8 in the third simulation. Distributions of c-axes orientations obtained at the end of each of the three simulations are shown in pole figures of Figs. 10 (a), (b) and (c), respectively, in which the surface is positioned at y=0 mm and y increases with depth.

Among the results shown in Fig. 10, the process of c-axes transition with depth is similar to the process in Figs. 8 and 9. However, results differ somewhat between

different growth rate anisotropies within the nucleus basal plane. Geometric selection of c-axes and preferred alignment occur closer to the surface for weaker anisotropy in the basal plane.

This is explained by the spaces opening up between dendrite arms, which are progressively larger for lager anisotropies, allowing other crystals to penetrate through these openings (Fig. 4). On the other hand, the circular-shaped grain does not have such a space, and it will block the growth from other nuclei. Hence, for less pronounced anisotropy in the basal plane, geometric selection of crystals is more effective. However, the transition depth between random and highly aligned c-axis fabrics does not change greatly, with the anisotropy of growth rate in the basal plane impacting geometric selection only in a minor way.

3.2 Effects of salt diffusion process and temperature gradient

In this section, the effects of temperature and salt on the formation of crystal textures in solidification processes of seawater are taken into account, and two simulations are performed under different temperature conditions in a two-dimensional approximation. In one simulation, the temperature in the volume is kept constant throughout the solidification process. In the other simulation, a temperature gradient in the volume evolves through cooling at the sea or ice surface. By comparing the results obtained from these simulations, we examine the effect of the temperature gradient on the growth process of polycrystalline ice in seawater. The conditions of the simulations are as follows.

A homogeneous seawater area is assumed for the simulation space which has dimensions of 50×150 mm^2. The upper edge of the space coincides with the sea surface and the space is filled with seawater with salinity of 35 ‰. Forty-five sites are randomly chosen near the upper edge of the simulation space as candidate positions for nucleation of crystallites. Nucleation is assumed to occur when the temperature at the candidate position becomes lower than the solidification temperature $\boldsymbol{T_s}$. Physical constants of ice and seawater used in the simulations are shown in Table 1.

In the first simulation, we assume that $\boldsymbol{g_0}$=0.01 mm/s, $\boldsymbol{R_{anisotropy}}$=0.3 and $\boldsymbol{n_s}$=6. The whole simulation space is kept at -4 °C during crystal growth. The results obtained are shown in Fig. 11. In the initial stage of crystal growth (Fig. 11 (a), (b)), crystallites grow mostly independently in stellar shape. Salt is discharged from the solidified area into the surrounding liquid volume, leading to the formation of a high-salinity layer. The degree of supercooling near the ice-seawater interface is small due to the high salinity and crystal growth becomes governed by the salt diffusion process. Once this condition is established, solidification is enhanced at crystal protrusions where salt diffusion is more rapid and planar growth is unstable. The protrusions are amplified with time and then dendrite arms are formed.

In confined volumes where diffusional transport is limited, salinity remains high. Thus, it becomes difficult for the concentrated brine to solidify in confined spaces, leaving liquid pockets within grains even if these are connected to low-salinity regions. This phenomenon is observed not only in the early stages of crystal growth when granular-shaped grains are formed near the surface but also in the stages when columnar-shaped grains are formed at the lower part of the sea ice (Figs. 11 (c)-(e)).

The geometry of the ice matrix within the columnar crystals is complicated, and a lamellar or platelet substructure is not observed.

Next, we introduce the effect of a temperature gradient into the simulation. We assume $\boldsymbol{g_0}$=0.1 mm/s and initial temperature in the whole simulation space is -1 °C. Then the sea surface is cooled and kept at -5 °C, while the bottom of the space is kept at -1 °C. In this condition a temperature gradient develops in the specimen with progress of time. The results obtained are shown in Fig. 12. We evaluate effects of temperature and salt on crystal growth by using degree of supercooling σ [%]:

$$\sigma = \frac{T_s - T}{T_s} \times 100 \,. \tag{8}$$

When σ is positive value, actual temperature T is lower than the solidification point T_s, and growth rate of the crystal increases with increase in σ.

In the early stages of crystal growth (Fig. 12 (a)), when ice crystals have not completely covered the sea surface, a layer in which there is a high degree of supercooling forms near the sea surface. Thus, growth rates of crystals are faster in the horizontal direction than in the downward direction, and crystal growth occurs mainly near the surface (Fig. 12 (b), (c)). Since the diffusivity of heat is higher in ice crystals than in seawater, the temperature in and around the crystals becomes lower (Figs. 12 (f)-(h)). Once the surface is covered with sea ice and the thickness of the sea ice increases (Fig. 12 (d)), temperature distribution in the horizontal direction becomes more uniform (Fig. 12 (i)). After that, fluctuation of temperature in the horizontal direction remains very

small and temperature at a deeper level decreases with time (Fig. 12 (j)).

Heat transport from the seawater under the sea ice to the ice surface (upper edge) is faster than the transport of salt away from the ice-seawater interface, and a mismatch of temperature and salt concentration occurs with respect to freezing point of the seawater under the sea ice. This results in the formation of a supercooled layer, so-called constitutional supercooled layer, in the seawater under the sea ice (Eicken, 2003). In the results of simulation (Fig. 12 (d), (e)), we also notice that the supercooled layer exists under the sea ice after the surface has been covered with sea ice.

Growth of ice crystals at the solid-liquid interface becomes unstable due to the effect of high-salinity layers, similar to the case shown in Fig. 11, and seawater that has high salinity is trapped within the ice crystals near the sea surface. However, in the zone of columnar crystals, the process by which brine is trapped differs from that shown in Fig. 11.

In the zone of columnar-shaped grains in Fig. 12, growth rates of most grains in the downward direction become almost the same due to the effect of quasi-uniform temperature distribution in the horizontal direction. Growth rates of thin ice arms protruding from irregularities at solid-liquid interfaces also become almost the same and growth directions also align. Areas of condensed seawater are left behind between the protrusions, and the tips of the protrusions keep advancing in the downward direction without connecting with each other due to the high-salinity seawater between them and high temperature around the tips (Fig. 12 (i), (j)). As a result, in the columnar ice zone, a lamellar-like structure that consists of brine layers and thin ice plates is formed in the

vertical direction (Fig. 12 (e), (k), (l)).

In the simulation model, buoyancy effect, surface energy and latent heat of solidification were ignored, and they would impact on formation process of actual sea ice polycrystals. However, in the present simulation, nuclei grew at the same growth rate and in the same direction due to the effect of a vertical temperature gradient that developed with cooling from the sea surface, and they finally formed columnar ice aligned vertically (Fig. 12 (k)), which is found in nature. Thus, we find that the vertical temperature gradient plays a significant role in the formation process of columnar ice structure.

4. Conclusion

We simulated the growth process of sea ice polycrystals in two and three dimensions by using a simple and numerically efficient simulation technique of Voronoi dynamics. The results are summarized as follows.

(1) The development of sea ice microstructure during ice growth was reproduced numerically. Simulations showed granular grain structures in the nucleation zone at the top of the volume and columnar grains at depth as a result of geometric selection and impingement of adjacent crystals.

(2) Geometrical selection of c-axes was more pronounced for simulations with a weak anisotropy in growth rate within the basal plane compared to highly anisotropic growth rates. However, the effect of the anisotropy on geometrical selection was modest.

(3) The effects of salt build-up at the ice-water interface, salt diffusion and temperature gradients were examined in different simulations. Crystals branched into thin ice plates during growth due to high-salinity layers developing at the solid-liquid interface. Growth directions of these thin ice plates were aligned and their growth rates were similar due to the equalizing effect of the temperature gradient. As a result, in columnar zone ice, a lamellar substructure of thin ice plates and brine layers which were parallel to the vertical direction were formed. The results show that vertical temperature gradient plays a significant role in the formation process of columnar ice structure.

Appendix: Procedure for the growth of artificial sea ice shown in Fig. 7.

First, a tank of 600 mm in width, 340 mm in height and 300 mm in depth was covered with insulating material on all four sides and on the bottom and was then filled with seawater obtained from the coast of Abashiri in Hokkaido, Japan. The tank was then cooled at -20 °C in a low temperature room. The sea ice had attained a thickness of 130 mm at 59.5 hours from the start of solidification of the seawater. An ice sample was taken from a position far from the sides of the tank. Fig.7 (a) and (b) show vertical cross-sectional views of the sea ice. The upper edge of the Fig.7 (a) corresponds to the top face of the sea ice and Fig.7 (b) is texture under the texture shown in Fig.7 (a). Fig.7 (c) shows a horizontal cross-sectional view at 115 mm from the top face. Fine or coarse-grained texture near the four sides of each photo is reinforcing material that was introduced during the process of making thin sections, and it is ice made of fresh water.

References

Assur, A,. 1958. Composition of sea ice and its tensile strength, Proceedings of the arctic sea ice conference. Easton, pp. 106-138.

Cole, D.M., 2001, The microstructure of ice and its influence on mechanical properties. Eng. Fracture Mech., 68 pp. 1797-1822.

Cota, G. F., Prinsenberg, S.J., Bennett, E.B., Loder, J.W., Lewis, M.R., Anning, J.L., Watson, N.H.F., Harris, L.R., 1987. Nutrient fluxes during extended blooms of Arctic ice algae. Journal of geophysical research, 92, pp. 1951-1962.

Eicken, H., Krouse, H.R., Kadko, D., Perovich, D. K., 2002, Tracer studies of pathways and rates of melt water transport through arctic summer sea ice. Journal of geophysical research, 107(C10), pp. 1-20.

Eicken, H., 2003. Growth, Microstructure and Properties of Sea Ice, In: Thomas, D.N., Dieckmann, G.S. (Eds.), Sea Ice: An Introduction to its Physics, Chemistry, Biology and Geology. Blackwell, Oxford, pp. 22-81.

Freitag, J., Eicken, H., 2003. Meltwater circulation and permeability of arctic summer sea ice derived from hydrological field experiments. Journal of glaciology, 166, pp. 349-358.

Golden, K.M. Ackley, S.F., Lytle, V.I., 1998. The percolation phase transition in sea ice. Science, 282, pp. 2238-2241.

Golden, K. M., Eicken, H., Heaton, A. L., Miner, J., Pringle, D. J., Zhu, J., 2007, Thermal evolution of permeability and microstructure in sea ice. Geophysical research letters, 34, pp. 1-6.

Gow, A.J., 1986, Orientation textures in ice sheets of quietly frozen lakes, Journal of crystal growth, 74, pp. 247-258.

Kawano, Y., Ohashi, T., 2006a. Numerical simulation for development of polycrystal microstructure of sea ice and brine formation by salinity concentration. Proc 21st Int. Symp. on Okhotsk sea & sea ice, pp. 95-98.

Kawano, Y., Ohashi, T., 2006b. Numerical simulation of development of sea ice microstructure by Voronoi dynamics technique. Proc. 18th IAHR Int. Symp. on ice, 2, pp. 97-103.

Lofgren, G. and Weeks, W.F., 1969, Effect of growth parameters on substructure spacing in NaCl ice crystals, Journal of Glaciology, 8(52), pp. 153-164.

Moslet, P. O., 2007, Field testing of uniaxial compression strength of columnar sea ice. Cold Regions Science and Technology, 48, pp. 1-14.

Nakao, M. and Sinha, N.K., 1984, A note on brine layer spacing of first-year sea ice, Atmosphere-Ocean, 22(2), pp. 193-206.

Noda, H., Von der Eerden, J. P., Furukawa, Y., 2004. A clear observation of crystal growth of ice from water in a molecular dynamics simulation with a six-site potential model of H_2O, Journal of crystal growth. 266, pp. 297-302.

Ohashi, T., Sasaki, M., Yoshimura, Y., 2004. Proc. 19th Int. Symp. on Okhotsk sea & sea ice, pp. 180-185.

Okagaki, O., 1998. Conduction of heat (Netsu Dendo), In: Nobuhiro S. (Ed.), Engineering of heat transmission (Dennetsu Kogaku). Morikita press (in Japanese).

Sasaki, M., 2003, Personal communication.

Shibkov, A.A., Golovin, Yu.I., Zheltov, M.A., Korolev, A.A., Leonov, A.A., 2003, Morphology diagram of nonequilibrium patterns of ice crystals growing in supercooled water, Physica A, 319, pp. 65-79.

Shimada, W., Furukawa, 1997. Y., Pattern formation of ice crystals during free growth in supercooled water. J. Phys. Chem. B, 101, pp. 6171-6173.

Schulson, E.M., 1999, The structure and mechanical behavior of ice. JOM, 51(2), pp. 21-27.

Timco, G.W., Frederking, R.M.W., 1990, Compressive strength of sea ice sheets. Cold Regions Science and Technology, 17, pp. 227-240.

The Japan society of mechanical engineers (Ed.), 2003. Data Book of heat transmission (Dennetsu Kogaku Shiryo). The Japan society of mechanical engineers (in Japanese).

Toba, Y., Kaimen kyokai katei, 1970 In: Masuzawa, J. (Ed.), Physical oceanography (Kaiyo butsuri). Tokai univ. press, Tokyo, pp. 145-263 (in Japanese).

Weeks, W.F. and Ackley, S.F., 1982. The growth, structure and properties of sea ice. CRREL Monograph.

Weeks, W.F. and Wettlaufer, J.S., 1996, Crystal orientations in floating ice sheets. In: Arsenault, R.J. et al. (Editors), The Minerals, Metals & Materials Society, pp.337-350.

Wettlaufer, J.S., 1992, Directional solidification of salt water: deep and shallow cells. Europhysics Letters, 19(4), pp.337-342.

Yokoyama, E., Sekerka, R.F., 2000. Growth trajectories of disk crystals of ice growing from supercooled water. J. Phys. Chem. B, 104, pp. 65-67.

Fig. 1. Schematic illustration of Voronoi dynamics technique.

Fig. 2 Schematic illustration of discharge of salt from a newly solidified cell. All of the discharged salt is distributed equally to neighboring liquid cells.

Fig. 3. Local coordinate system x_0-y_0-z_0 defined for each of the nuclei.

Fig. 4. Shapes of crystal nuclei in the 3-dimensional growth model when growth rate parameters are changed. It is assumed that $\boldsymbol{n}_s$=6.

Fig. 5. Development process of ice crystals from the surface obtained by numerical simulation.

Fig. 6. Cross-sectional views of crystal structure obtained from Fig.5 (f). (a) and (b) are vertical cross sections and (c) is a horizontal cross section.

Fig. 7. Artificial sea ice crystal when cooling temperature is -20 °C (Sasaki, 2003). (a) and (b) are vertical cross sections. (a) is a structure near the surface and (b) is a structure near the bottom of the ice. (c) is a horizontal cross section.

Fig. 8. Pole figures showing distribution of c-axes orientations of simulated sea ice at different depth levels. 0 mm is the top face of the ice crystal. Each dot in the figure indicates c-axis orientation. Dots with a darker color indicate larger cross-sectional area.

Fig. 9. Pole figures showing distributions of c-axis orientation of real sea ice (Weeks and Ackley, 1982). 0-5 mm is the top face of the ice crystal. Dark color region indicates accumulation of c-axis orientations.

Fig. 10. Distributions of c-axis orientation of sea ice obtained in the simulations. 0 mm is the top face of the ice crystal. Each dot in the figure indicates c-axis orientation. Dots with a darker color indicate larger cross-sectional area.

Fig. 11. Results obtained when a temperature gradient does not exist. (a)-(e) are salinity distributions and (f) shows crystal structure.

Fig. 12. Results obtained when a temperature gradient exists in the specimen. (a)-(e) are distributions of degrees of supercooling of seawater, (f)-(j) are temperature distributions, (k) shows crystal structure and (l) shows salinity distribution.

Table 1. Physical constants used in the present simulations (Toba, 1970; Okagaki, 1998; Data Book of Heat Transmission, 2003). For the density of seawater, however, we used an approximated value, i.e., value of fresh water.

	Ice	**Seawater**
Diffusion coefficient of salt *D* [m^2/s]		**6.8×10^{-10}**
Specific heat *c* [J/kgK]	**2040**	**4217**
Diffusivity of heat *a* [m^2/s]	**1.17×10^{-6}**	**0.139×10^{-6}**
Density ρ [kg/m^3]	**916.8**	**1000**

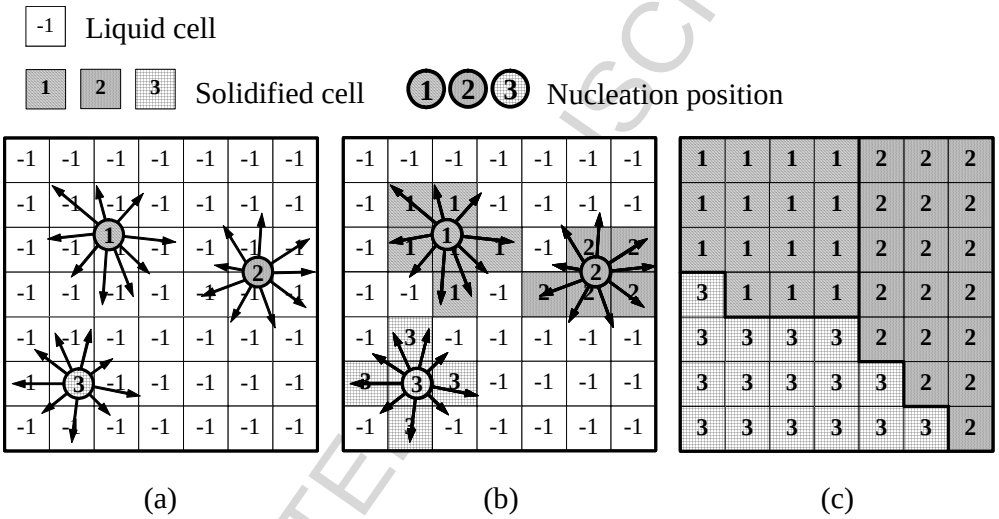

Fig. 1. Schematic illustration of Voronoi dynamics technique.

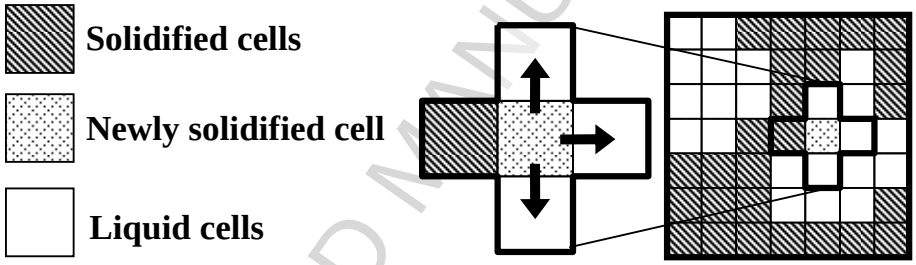

Fig. 2 Schematic illustration of discharge of salt from a newly solidified cell. All of the discharged salt is distributed equally to neighboring liquid cells.

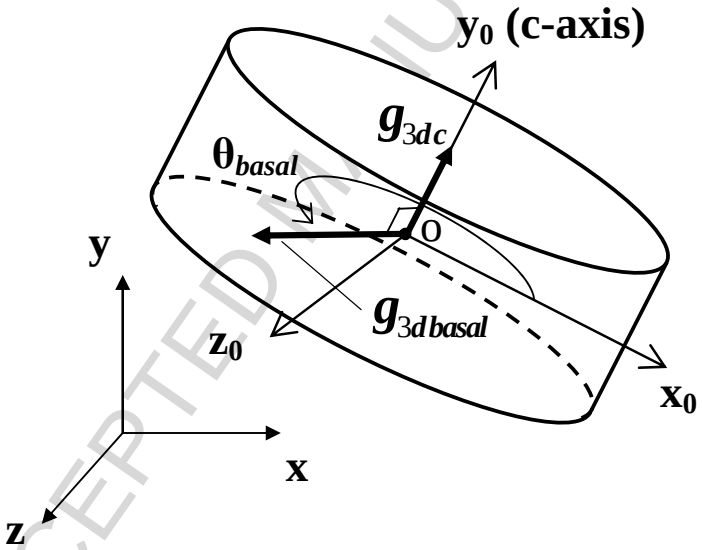

Fig. 3. Local coordinate system x_0-y_0-z_0 defined for each of the nuclei.

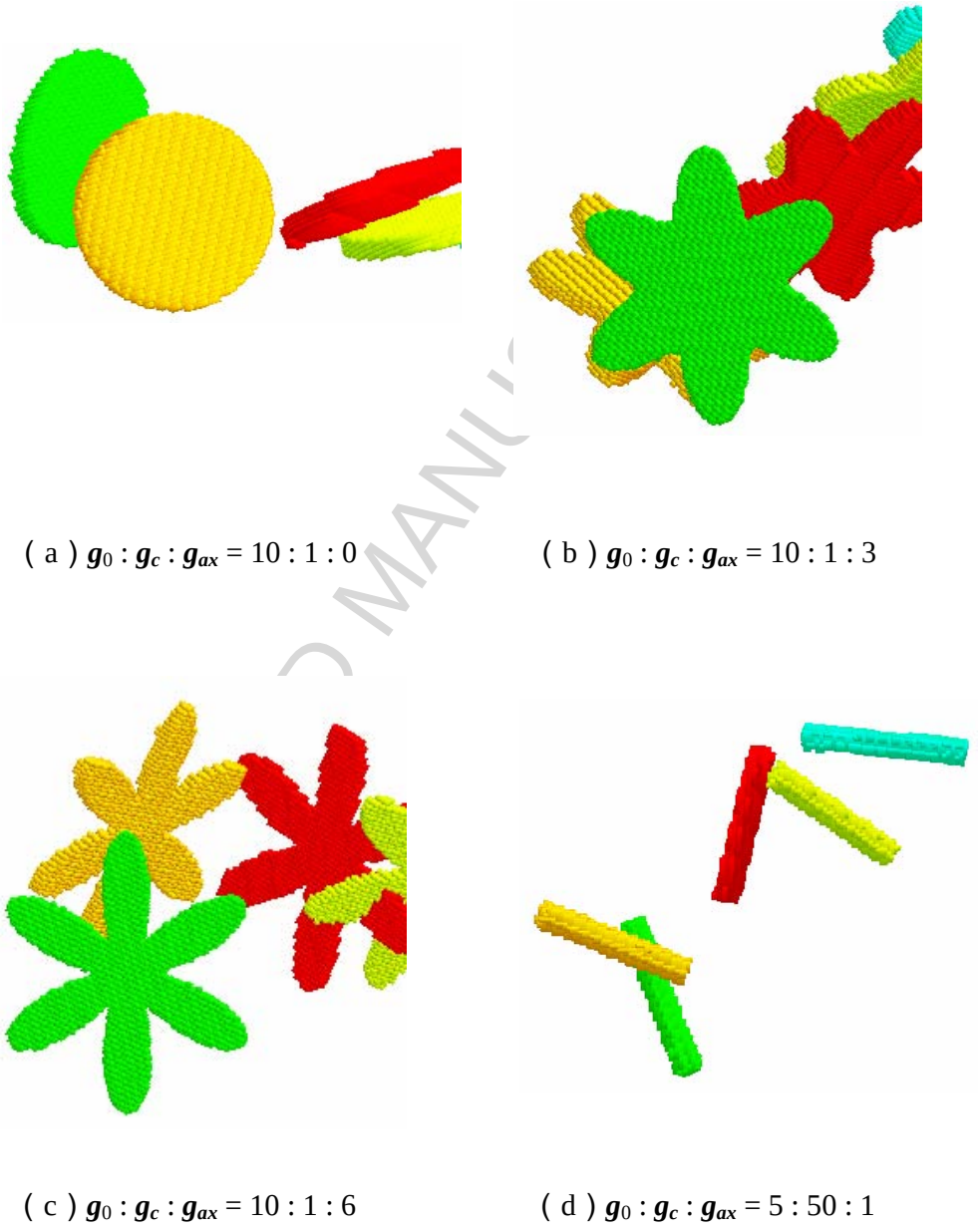

(a) $g_0 : g_c : g_{ax} = 10 : 1 : 0$ (b) $g_0 : g_c : g_{ax} = 10 : 1 : 3$

(c) $g_0 : g_c : g_{ax} = 10 : 1 : 6$ (d) $g_0 : g_c : g_{ax} = 5 : 50 : 1$

Fig. 4. Shapes of crystal nuclei in the 3-dimensional growth model when growth rate parameters are changed. It is assumed that n_s=6.

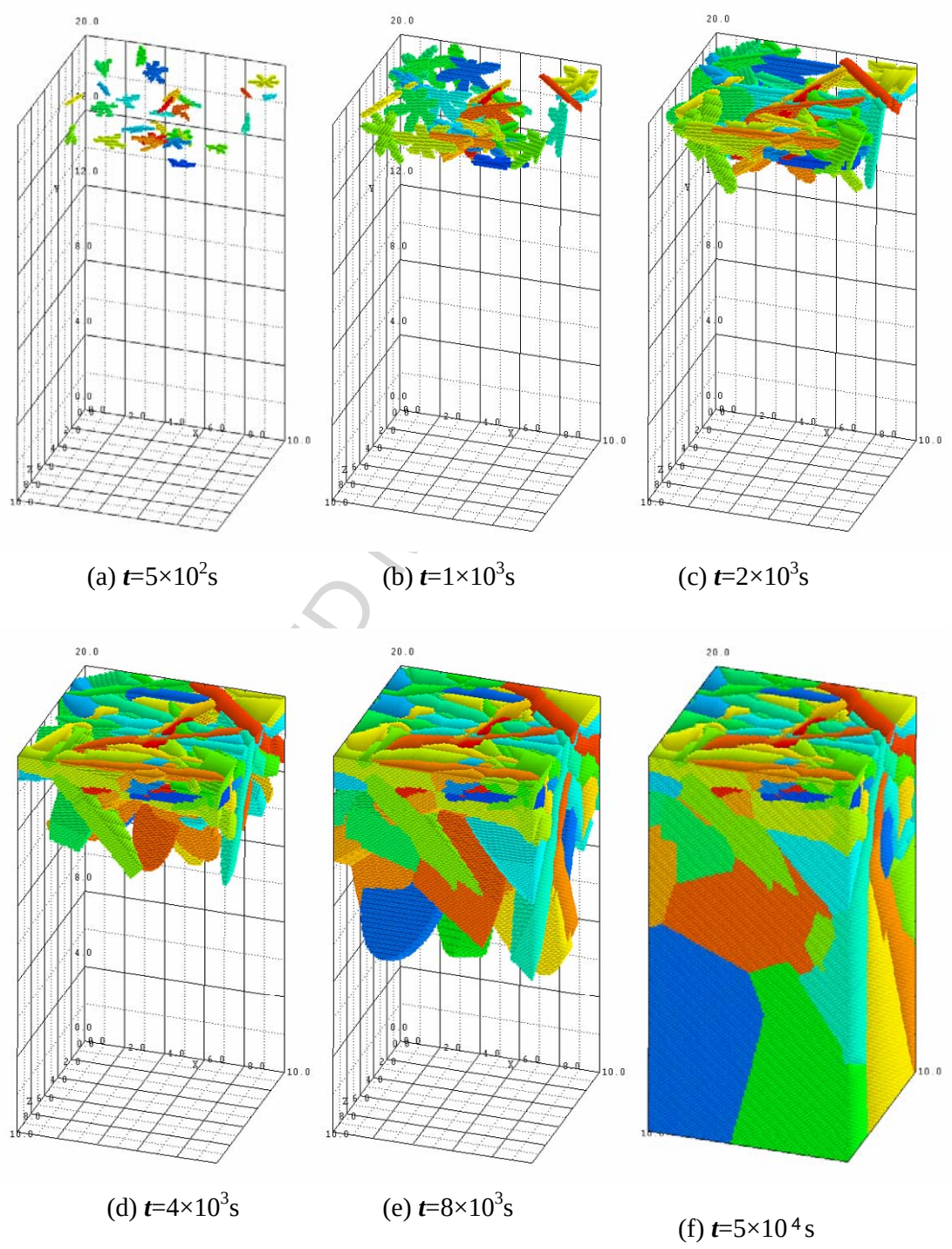

(a) t=5×10^{2}s (b) t=1×10^{3}s (c) t=2×10^{3}s

(d) t=4×10^{3}s (e) t=8×10^{3}s (f) t=5×10^{4}s

Fig. 5. Development process of ice crystals from the surface obtained by numerical simulation.

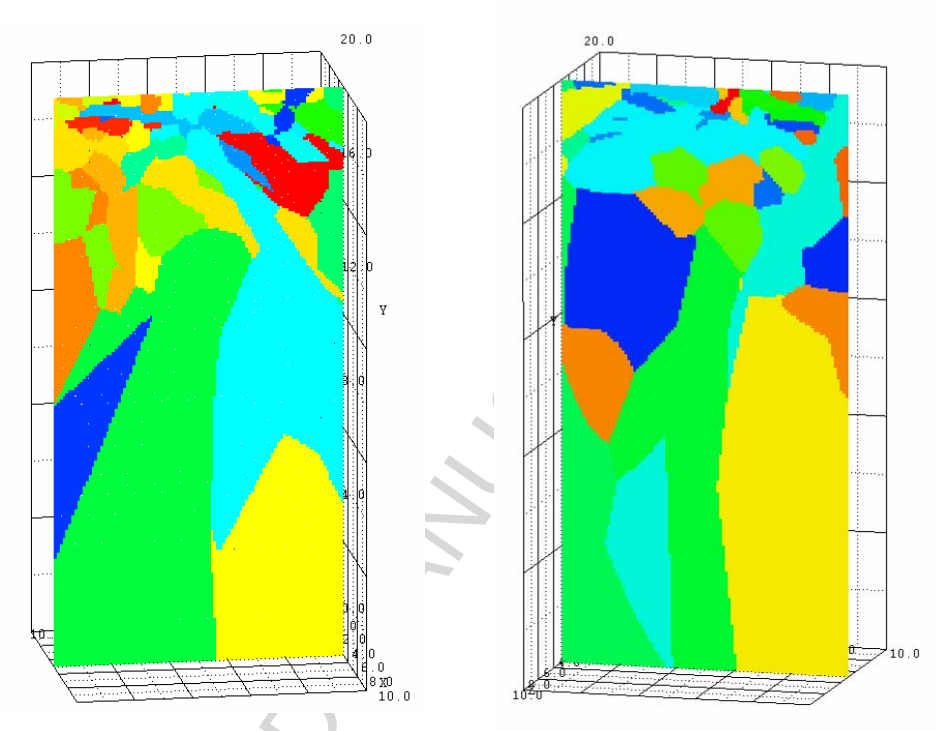

(a) x=50mm (b) z=50mm

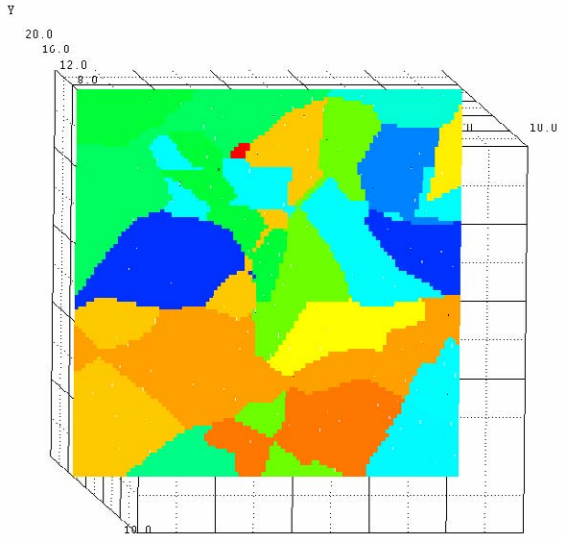

(c) y=50mm

Fig. 6. Cross-sectional views of crystal structure obtained from Fig.5 (f). (a) and (b) are vertical cross sections and (c) is a horizontal cross section.

(a) (b)

(c)

Fig. 7. Artificial sea ice crystal when cooling temperature is -20 °C (Sasaki, 2003). (a) and (b) are vertical cross sections. (a) is a structure near the surface and (b) is a structure near the bottom of the ice. (c) is a horizontal cross section.

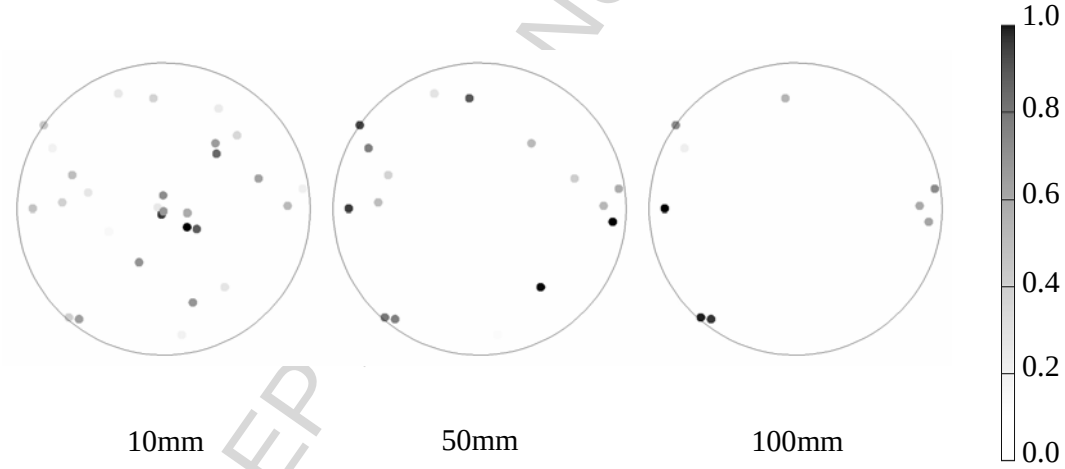

Fig. 8. Pole figures showing distribution of c-axes orientations of simulated sea ice at different depth levels. 0 mm is the top face of the ice crystal. Each dot in the figure indicates c-axis orientation. Dots with a darker color indicate larger cross-sectional area.

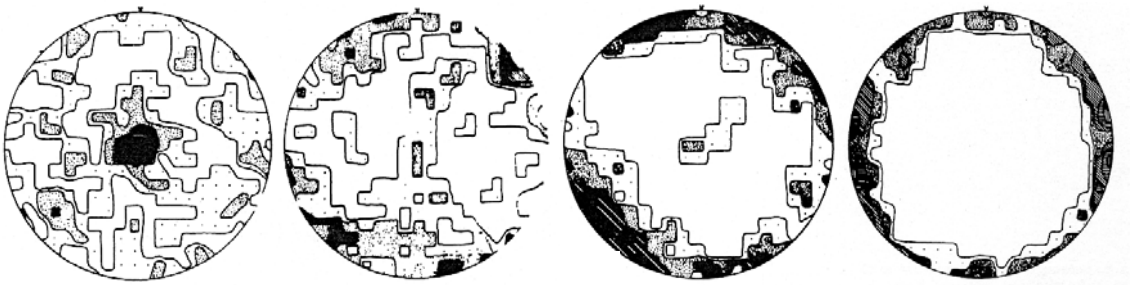

Fig. 9. Pole figures showing distributions of c-axis orientation of real sea ice (Weeks and Ackley, 1982). 0-5 mm is the top face of the ice crystal. Dark color region indicates accumulation of c-axis orientations.

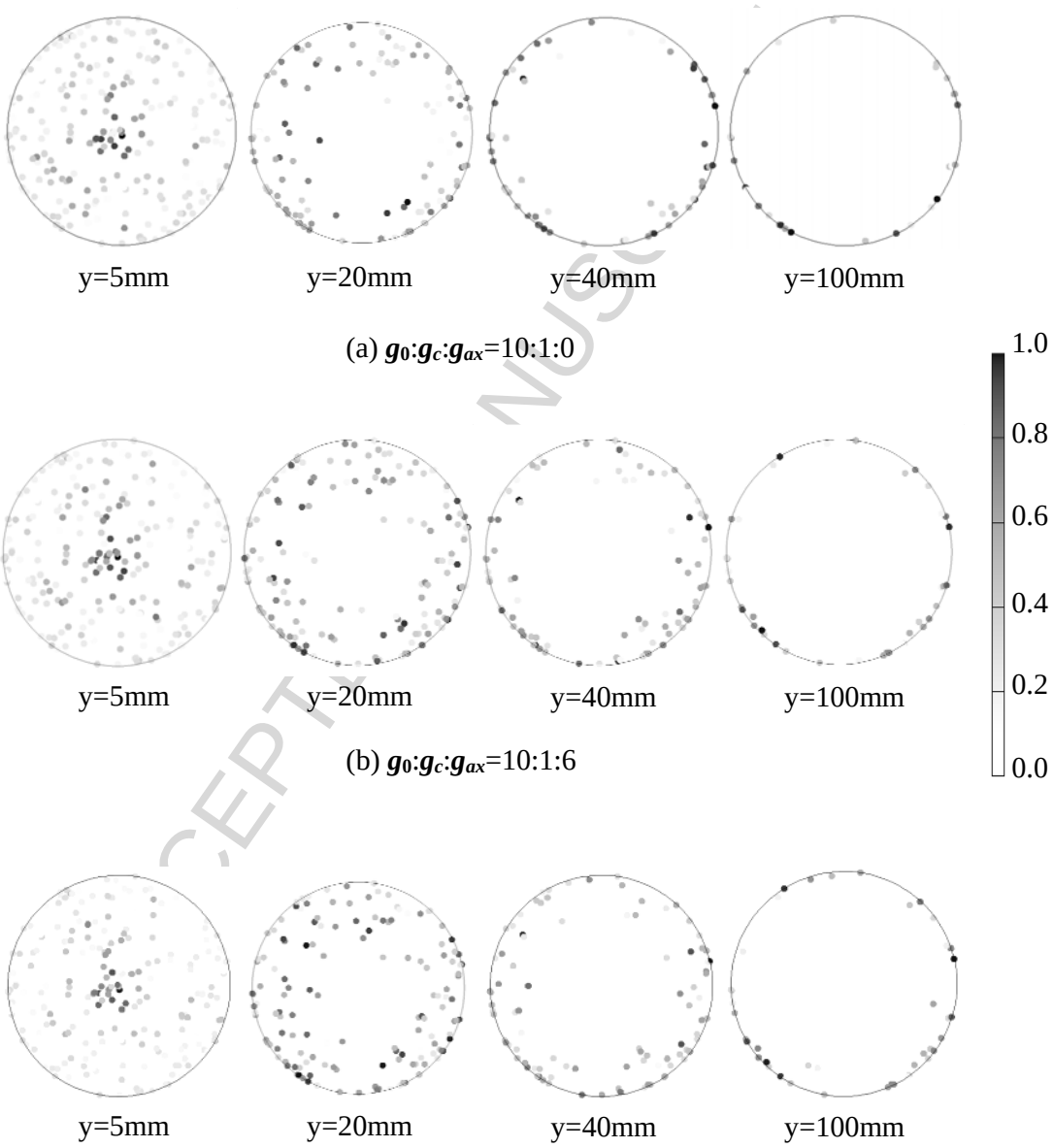

Fig. 10. Distributions of c-axis orientation of sea ice obtained in the simulations. 0 mm is the top face of the ice crystal. Each dot in the figure indicates c-axis orientation. Dots with a darker color indicate larger cross-sectional area.

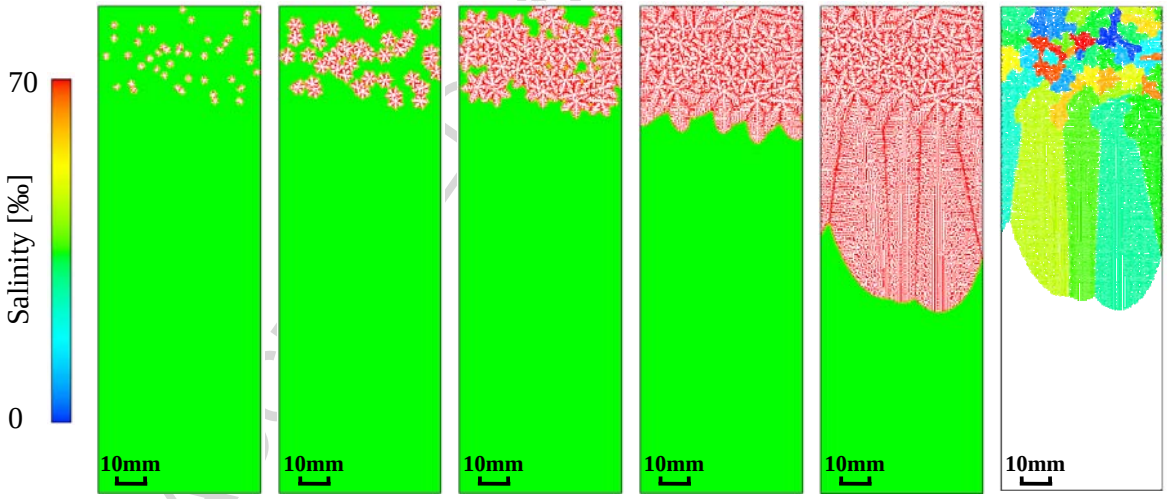

Fig. 11. Results obtained when a temperature gradient does not exist. (a)-(e) are salinity distributions and (f) shows crystal structure.

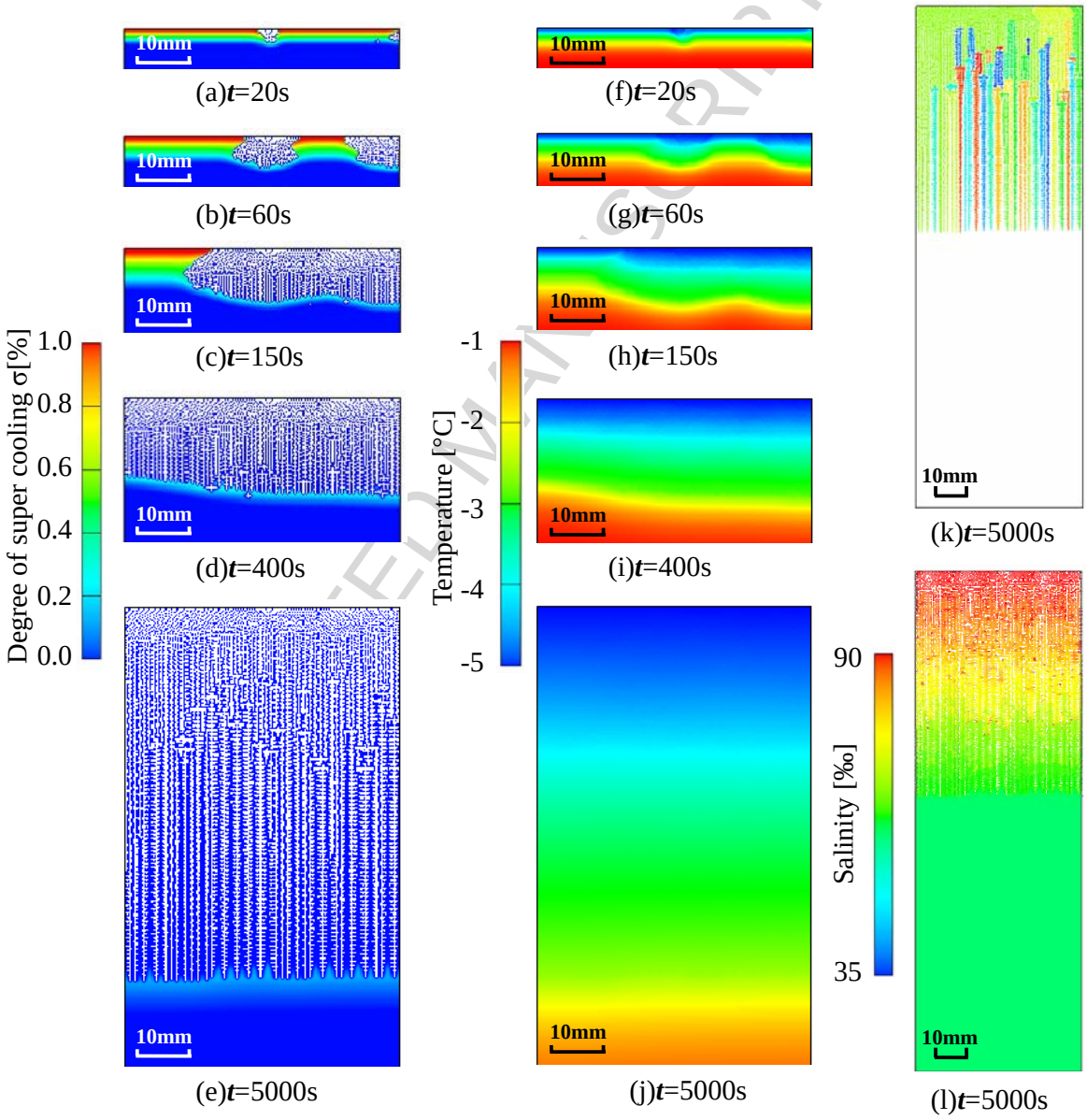

Fig. 12. Results obtained when a temperature gradient exists in the specimen. (a)-(e) are distributions of degrees of supercooling of seawater, (f)-(j) are temperature distributions, (k) shows crystal structure and (l) shows salinity distribution.